LL

The JET Team
presented by A Tanga

First Results with the Modified JET

JOINT EUROPEAN TORUS **JET**

First Results with the Modified JET

The JET Team
presented by A Tanga

JET Joint Undertaking, Abingdon, Oxon, OX14 3EA, UK.

First Results with the Modified JET

The JET Team[1]
(presented by A Tanga)

JET Joint Undertaking, Abingdon,
Oxfordshire, OX14 3EA, UK.

Abstract: JET was extensively modified in the 1992/93 shutdown. The new pumped divertor and many new systems were brought into operation early in 1994. Operations have progressed to 4MA plasma current and, with substantial additional heating, H-mode confinement results confirm the expected scaling. The high power handling capability of the pumped divertor with sweeping is estimated at 20MW for 20s. H-mode plasmas have large Type I ELMs. With lower hybrid heating alone, 2MA full current drive has been achieved with good efficiency, and with ICRF power, effective heating and direct electron heating have been demonstrated.

1. JET modifications

During the 1992/93 shutdown, JET [1] was extensively modified. Inside the vessel, the new pumped divertor was installed and, as a consequence, the layout of the whole vessel was modified to accommodate it [2].

The neutral beam (NB) injection system was upgraded to 22MW. New ion cyclotron resonance frequency (ICRF) antennae, with power capability up to 20MW, and with an enhanced fast wave current drive facility has started operation. A new lower hybrid (LH) wave system with power up to 10MW has also started. A new computer system for machine control and data acquisition was installed and made operational. A new plasma position control and machine protection system were also implemented. Inside the vessel, new saddle coils for disruption control and TAE excitation have been installed. In addition, most diagnostics had to be relocated due to the new in-vessel lay-out and 22 new diagnostics were added, providing information both on the divertor and on the main plasma.

1.1 In-vessel layout

A cross-section of the vessel with all its new features is shown in Figure 1. In particular, there are four divertor coils, which are individually powered, on the bottom of the vessel. Water-cooled divertor target plates sit on top of these coils. At present, graphite fibre-reinforced target plates are used, but later experiments are planned using beryllium target plates. Close to the outer divertor coil is the cryopump structure, which is cooled by liquid nitrogen and liquid helium. On the outer part of the vessel, the cross-section of the new ICRF antennae and new poloidal limiters are visible .
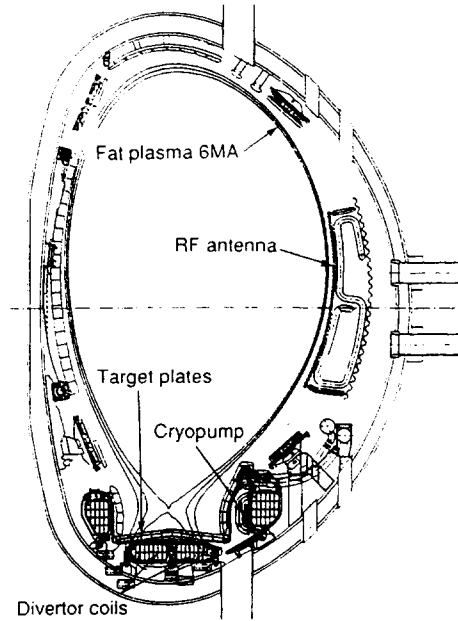
---

[1] See Appendix I

Figure 1. Divertor configuration for the new phase of JET

Figure 2 shows the inside of the vessel at the end of the shutdown. At the bottom of the vessel is the divertor with graphite tiles. The divertor coils and the cryopump are just visible hidden beneath the layer of graphite tiles. Two ICRF antennae, one LH launcher and the top and bottom saddle coils are evident. Also visible is one of the heads of the beryllium evaporators used for vessel conditioning.
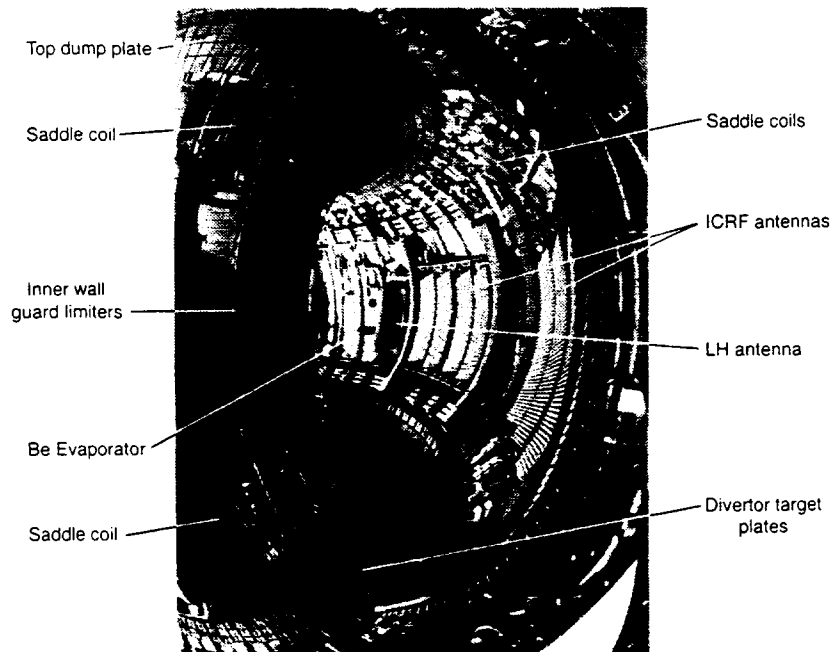

Figure 2. Inside the JET vessel

1.2 Additional heating

The installed neutral beam power capability is set out in Table I, which shows the variation with ion source used in the two injectors.

Table I: NBI Installed Power Capability

Ion	Power	Voltage
D_2	22MW	85kV/140kV
H_2	10.4MW	70kV/110kV
^3He	19MW	80kV/155kV
^4He	18MW	80kV/120kV
T_2	12MW	160kV
D_2	12MW	85kV

Using one injector at 85kV accelerating voltage and the other one at 140kV, 22MW of neutral beam power is available in deuterium. The total power in hydrogen is 10MW, while in He^3, a maximum power of 19MW is available or, in He^4 a maximum of 18MW. For the forthcoming D-T experiments, it is planned to have one injector in tritium with a power of 12MW at 160kV and the other in deuterium with a power of 12MW at 85kV, giving a total power of 24MW. The vertical direction of the beams can be adjusted on a shot-to-shot basis in order to optimize the deposition profile according to plasma geometry. New injection duct protections have been installed, which allows long pulse operation, and operation at low plasma current. The injectors have been equipped with high currents sources and since the start of operations, 17MW power has been achieved routinely.

The new ion cyclotron resonance frequency (ICRF) antennae are made of four straps for enhanced fast wave current drive capability. The coupling to the RF power to the plasma behaves as expected and 9MW power has been coupled using automatic matching and phasing. The new Lower Hybrid (LH) wave system uses a new launcher, and includes a cryopump which allows high-power long-pulse operation. It is powered by 24 klystrons and has a power capability of 10MW, of which 5MW has been routinely coupled to the plasma during early 1994.

1.3 Diagnostics

The full list of the 22 new diagnostics for divertor studies is presented in Table II. Special mention is made of certain new developments, as follows:
1. a new neutral particle analyser (NPA) is operational, which measures MeV ions (produced either by ICRF heating or as fusion products). A schematic cross-section is shown in Figure 3;
2. a neural network technique has been applied to produce real-time temperature and rotation profile of ions. Figure 4 shows a comparison between the time evolution of ion temperature achieved by the standard method compared with that achieved by neural network analysis techniques.

Table II. List of New JET Diagnostics

| Diagnostic	Purpose
Bolometry of divertor region	Power balance of divertor plasma
In-vessel bolometer array	Time and space resolved radiated power
Magnetic pickup coils	Plasma geometry in divertor region
Calorimetry of Mark I divertor targets	Power balance of divertor plasma
Fast ion and alpha-particle diagnostic	Space and time resolved velocity distribution
Lidar Thomson scattering	T_e and n_e profiles in divertor plasma
Microwave interferometer	$\int n_e dl$ along many chords in divertor plasma
Microwave reflectometer	Peak n_e along many chords in divertor plasma
E-mode reflectometer	Measurement of density profiles in edge and SOL
Compact soft X-ray cameras	MHD instabilities, plasma shape
Compact soft X-ray camera	Toroidal mode number determination
Electron cyclotron absorption	$n_e T_e$ profile along many chords in divertor plasma
14MeV neutron spectrometer	Neutron spectra in D-T discharges,
14MeV time-of-flight neutron spectrometer	ion temperatures and energy distributions
VUV spatial scan of divertor	Time and space resolved impurity densities
Toroidal view visible spectroscopy of divertor plasma from Octant No: 7 mid-plane	T_z and V_z, ion temperature and toroidal velocity of impurities
Poloidal view visible spectroscopy of divertor plasma using a periscope	Impurity influx, 2-D emissivity profile of lines
VUV and XUV spectroscopy of divertor plasma	Impurity influx, ionization dynamics
Langmuir probes in divertor target tiles	n_e and T_e in the divertor plasma
Fast pressure gauges	Neutral flow in divertor region
50kV lithium atom beam	Parameters of the scrape-off-layer plasma
Thermal helium beams	n_e and T_e in the divertor plasma
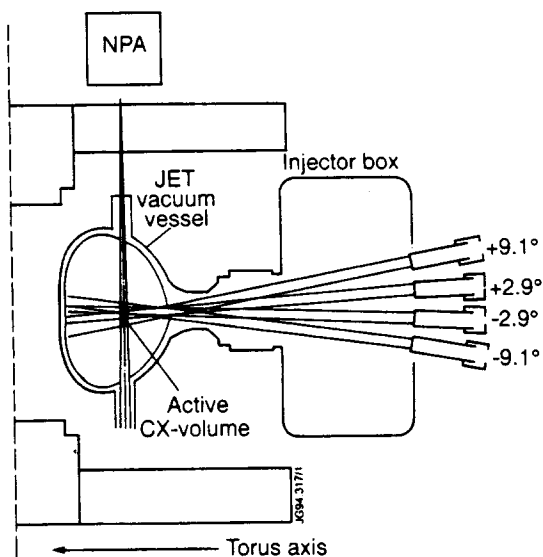
Figure 3. NPA for measurement of
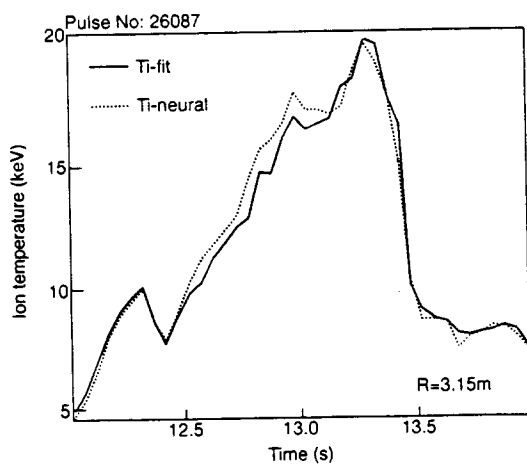MeV energy ICRF driven minority ions
and fusion products

Figure 4. Neural network techniques:
application to real-time ion temperature
and rotation profiles

4

Among the new systems about to become operational are the pellet injectors, the TAE excitation system, and the disruption feedback system using the in-vessel saddle coils.

2. Development of operations

Operation restarted at the end of January 1994. Before the production of reliable plasmas, the new plasma control system was commissioned. The modified additional heating systems were brought into operation and energies up to 90MJ were injected in a single pulse. To accommodate this power within the divertor, sweeping of the strike points across the target plates has been used routinely and this has proved to be highly effective in reducing the local power load. The development of the plasma current has progressed up to 4MA and H-modes using NB injection up to 17MW have been achieved routinely .

2.1 Machine conditioning

The operating temperature of the vessel is 250°C. As a routine cleaning technique, Glow Discharge Cleaning (GDC) and Be evaporation are used daily. For divertor tile conditioning, helium discharges and high power heating have been used, raising the surface tile temperature to 1,200°C. As a result of this conditioning, the plasma effective charge, Z_{eff}, was in the range 1.5 to 3. Values of the density limit were in line with previous results.

The in-vessel cryopump has been used, cooled with liquid nitrogen, which effectively traps carbon and oxygen impurities.

2.2 Development of plasma current

Equilibrium of a 4MA discharge at 3.4T toroidal field is shown in Figure 5.
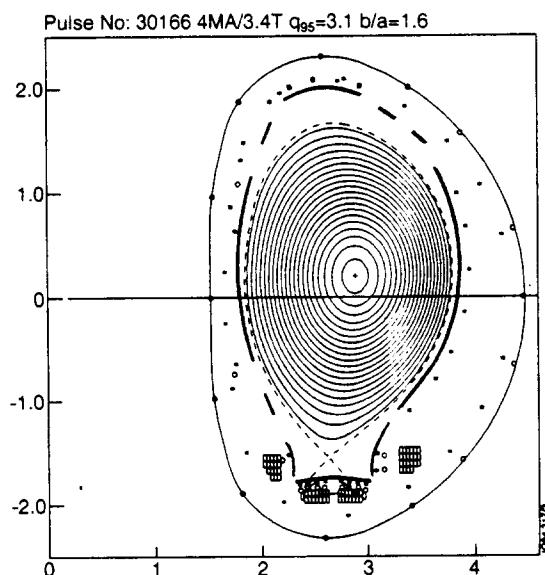

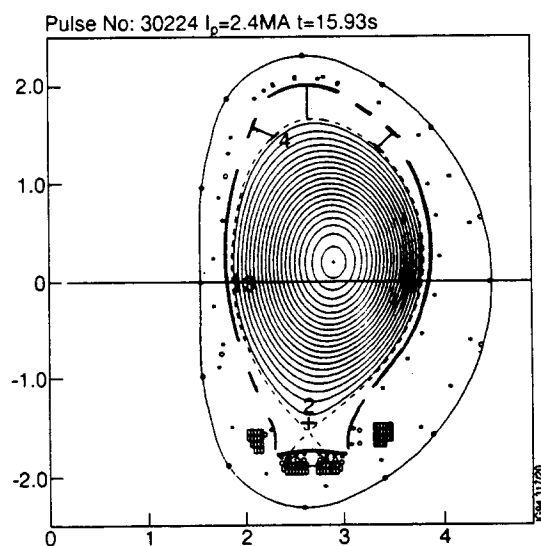Figure 5. 4MA equilibrium Pulse No: 30166 at 4MA/3.4T

Figure 6. Real-time plasma boundary measurements and control

4 MA plasma current operations were performed at full toroidal field (3.4T). The plasma had good clearance from both the outer and inner limiters. However, the safety factor, q_{95}, was 3.1, since the elongation had been limited to 1.65 in order to reduce potential forces in the event of a disruption. Thus, full use was not made of the volume available. The divertor configuration was formed at the end of the current rise, and a flat-top of 15s was achieved routinely.

2.3 Plasma control

Figure 6 shows the operation of the real-time plasma boundary measurement and control. This is a system which calculates the plasma boundary every 2ms and its signals are used to control the shape of the plasma. Five distances and positions are independently controlled: the outer gap; the top gap; the inner gap; and both the radial and vertical positions of the X-point.

A system for stabilization of the vertical plasma position, separate from the control of plasma boundary position, uses of a new amplifier, which is ten times faster than the previous one. The response time of the amplifier is 200µs, while the digital controller system of stabilization of vertical position samples with a period of 50µs.

Operation of the vertical stabilization system is shown in Figure 7. When the gain was switched off, the plasma, was vertically unstable, with a growth rate of 4ms and started to move upward with characteristic increasing speed. After 20ms, the gain is switched on again, and the stabilization system brings the plasma back to its original position. The controller required a large current to the amplifier to produce the stabilization of the plasma vertical position.
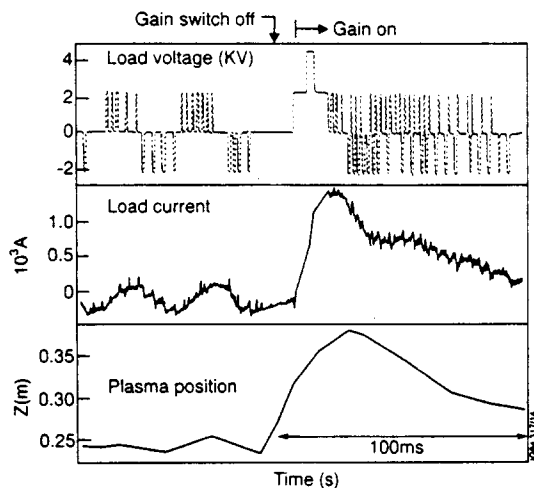

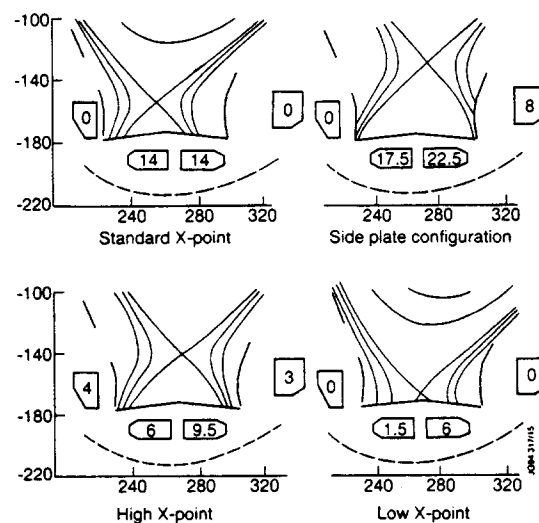Figure 7. Stabilization of plasma vertical position

Figure 8. X-Point configurations

2.4 Divertor configurations

With four divertor coils, a range of X-point configurations has been produced, as shown in Figure 8. Using current only in the bottom two divertor coils at 14kA each, in a 2MA plasma, the "standard X-point configuration" was produced, which had a X-point height above the target plates of ~25 cm. However, by using the inner and outer divertor coils as

6

well, the height of this point could be raised to 35 or 40cm and this is called the "high X-point configuration". By making use of the shaping coils outside the vessel in combination with the bottom divertor coils, a configuration in which the X-point is much closer to the bottom divertor target plates has been produced. This position, in which the X-point practically coincides with the surface of the tiles, is called the 'low X-point configuration".

Using a combination of both the divertor coils and outer divertor coils, a configuration in which the power load and particle load, instead of being directed to the bottom target plate, was directed to the side target plate. This is called the "side-plate configuration", which could have superior divertor capability.

2.5 Sweeping and divertor power handling capability

Sweeping of the strike points over the target plates is necessary to accommodate high heating power on the divertor. This means moving the X-point radially only by a few centimetres. This X-point movement is translated into a larger movement of the strike points on the target plates. The maximum sweeping range over the target plate is ~30cm. Sweeping produces reduced local heat loads by factors of 5 to 10. It has been estimated that, by making use of the full surface area, the maximum energy which can be accommodated in the divertor is ~400MJ (ie. 20MW for 20s). A typical flux plot with sweeping is shown in Figure 9, in which the sweeping frequency is 4Hz. It has been found that sweeping the X-point is compatible with ICRF (see Figure 10) and LH coupling.
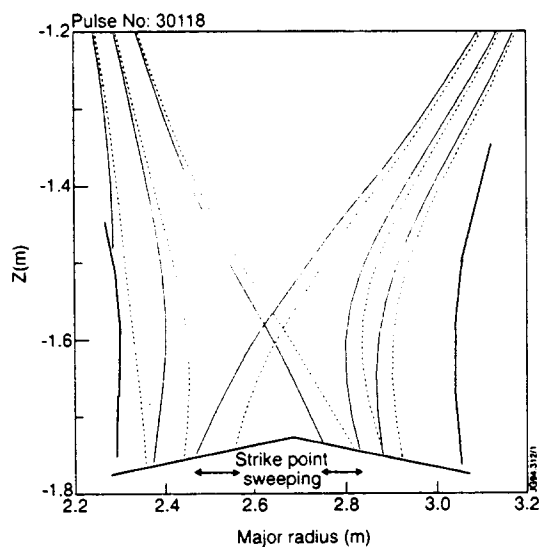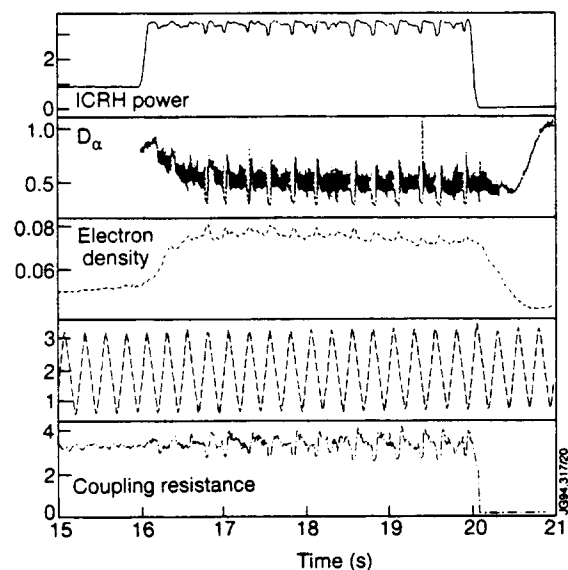

Figure 9. Sweeping of X-point

Figure 10. ICRF heating with coupling resistance feedback

With ICRF heating, the coupling resistance feedback system has been used. The outer gap of the plasma was controlled by using the value of the coupling resistance as a reference parameter (in this case 3.5Ω). The sweeping was in operation, seen from the modulation of the current of the divertor coil, while the ion cyclotron power was kept constant. The value of the coupling resistance changed slightly and this was due only to the incipient transition from H to L-mode during the heating (D_α trace). The effect of sweeping in reducing the heating of the target plates is shown in Figure 11. Initially the divertor coil current was kept

This figure indicates the radial profile of the ion saturation current both for the inner and outer divertor legs, showing the profiles for a plasma which was first attached and then detached. There is a strong reduction in ion saturation current of the detached plasma compared with the attached one, both on the inner and outer legs. For detached plasmas, the maximum value of the ion saturation current peaks far away from the position of separatrix, giving an indication of temperature reversal. This measurement has been confirmed by CCD camera and by D_α observations.

3. H-mode results

H-mode confinement has been achieved for plasma currents up to 4MA. The global confinement time is consistent with the JET-DIII-D H-mode scaling (ie. twice L-mode confinement). The power threshold depends on plasma density and toroidal field, as in the past. However, large Type I ELM's were present much more prominently than in previous experiments, and were always present in high power discharges. So far, ∇B ion drift was directed toward the X-point, but experiments will be carried out to check behaviour with the drift in the reverse direction.

3.1 H-mode behaviour and confinement

The time evolution for typical H-mode signals for a 4MA plasma are shown in Figure 13. Characteristically, there is a short ELM-free period in which the stored energy increases continuously and the plasma density increases similarly. Plasma stored energy is plotted versus heating power and compared with the JET/DIII-D H-mode scaling in Figure 14.
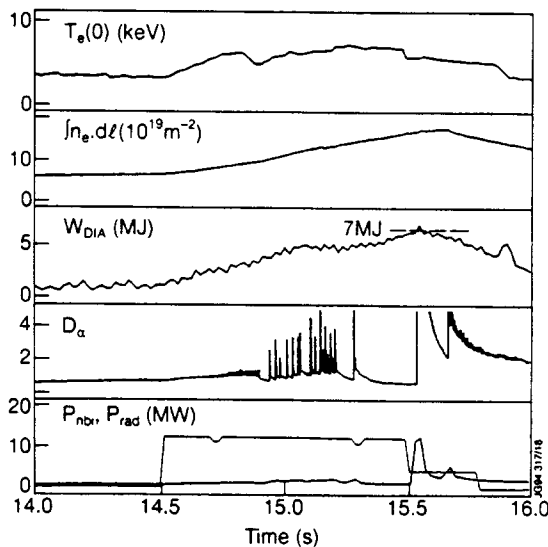

Figure 13. 4 MA H-mode (NBI Power 12 MW:
global confinement is twice L-mode:
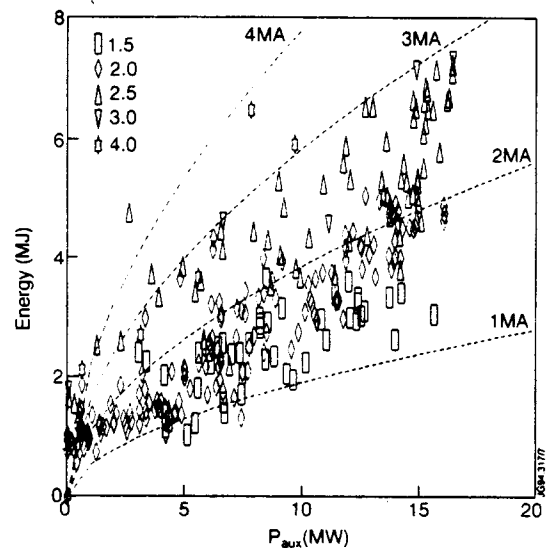and $R_{dd} = 1.2 \times 10^{16} s^{-1}$)

Figure 14. Plasma stored energy versus
heating power
(ELMy H-mode)

The dotted lines labelled 1, 2, 3 and 4MA refer to the values deduced from JET/DIII-D H-mode scaling laws. It is apparent that the confinement time of the 1994 JET H-mode is approximately in agreement with this scaling. The power threshold for the H-mode is similar to previous JET results [2] and this is shown in Figure 15. The H-mode points, calculated at the time of the L-H transition, are plotted in the space defined by the applied

8

NB power and the parameter product n_eB_T. All 1994 H-mode results are within the same region as those defined by the results from the 1991/92 campaigns.

3.2 ELM's

In all the 1994 H-modes, after an initial dithering with a few Type III ELM's, an ELM-free phase took place. The duration of the ELM-free phase decreased with power and was followed by a series of Type I ELM's. The behaviour of ELM's was unaffected by X-point sweeping. The frequency of the Type I ELM's increased with power.
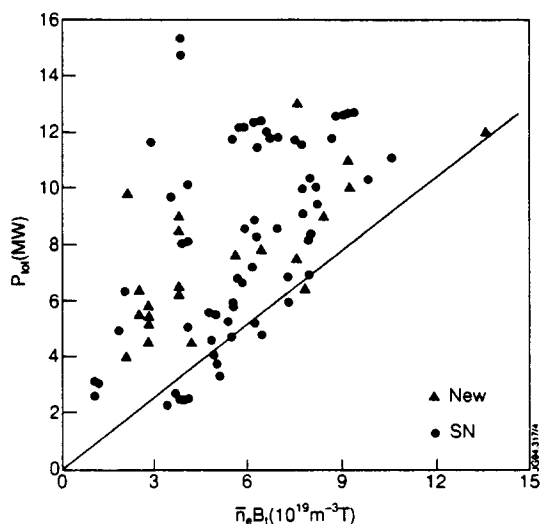

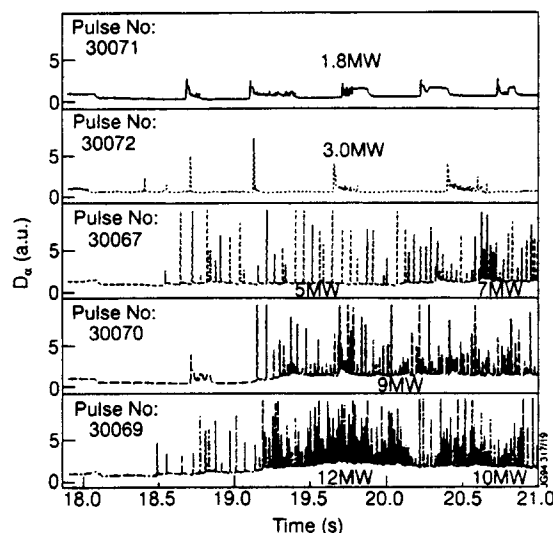Figure 15. H-mode power threshold

Figure 16. ELM's frequency increase with power

This increase in ELM's frequency with power is indicated in Figure 16, which shows a power scan for a series of plasma pulses with plasma current of 1.5MA and toroidal field of 1.4T. In the first pulse with 1.8MW, the NB power is just sufficient to produce some H-mode transitions, so there is some period in which the plasma stays in H-mode and then some in L-mode. At 3MW, the power was just above the threshold and then the ELM-free H-mode remained except for some few well spaced ELMs. By increasing the power to 5MW, to 7MW, and then to 9MW and to 12MW, the frequency of the ELM's increased further and further. Then, by reducing the power to 10MW the frequency decreased.

3.3 Hot-ion H- mode

The first hot ion H-mode regime has been achieved and an example is shown in Figure 17. The D-D reaction rate increased continuously during the H-mode phase up to $3 \times 10^{16} s^{-1}$. The ion temperature reached 17keV, the same as for the D-T experiments in 1991 [3].

4. Results of radio frequency studies

With lower hybrid power, full current drive was obtained up to currents of 2MA. High current drive efficiency has been achieved, showing a T_e dependence. Sawteeth activity was stabilised. With ICRF heating, direct electron heating by TTMP has been observed.

constant and then was modulated to produce the sweeping. The NB power was applied at constant power producing an H-mode transition with a short ELM free period followed by Type I ELM's.
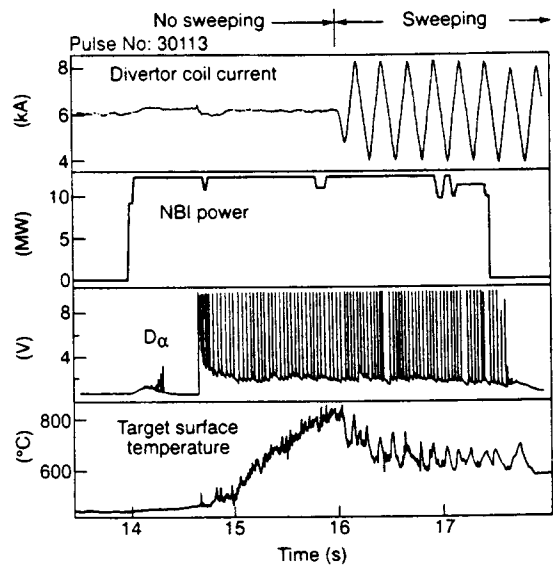

Figure 11. Effect of sweeping on target temperature

The effect of sweeping on the target temperature is shown in Figure 11. During the first non-swept part of the pulse, with the delay due to the plasma confinement time, the surface temperature of the target tiles increased with the characteristic dependence on the square root of time. Then, with the introduction of sweeping, the temperature decreased and became almost constant, demonstrating the effectiveness of the sweeping. Detachment of the divertor plasma in ohmic discharges has been observed, as shown in Figure 12.
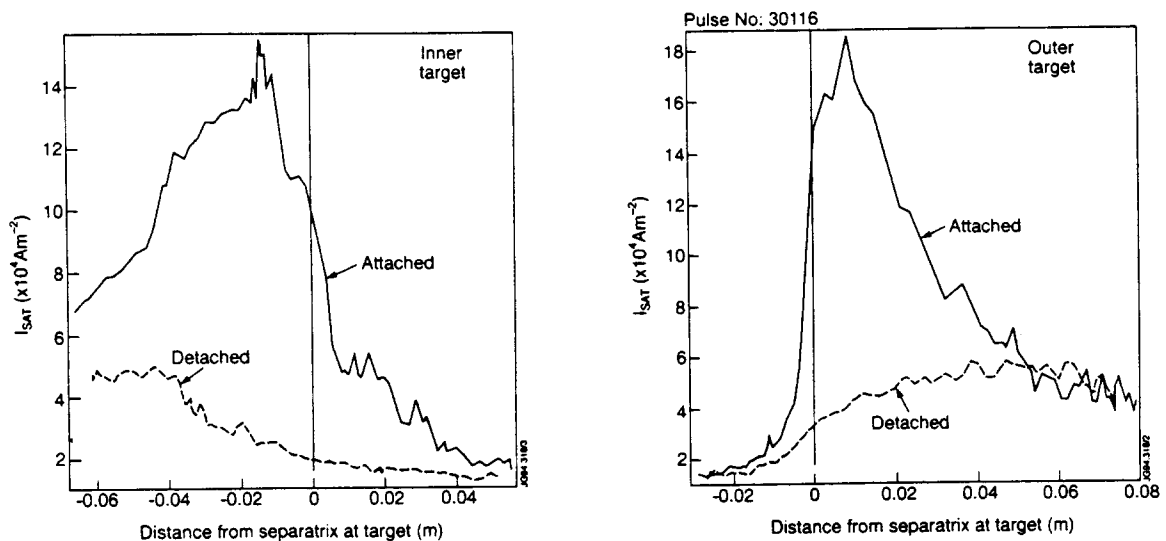

Figure 12. Detachment of divertor plasmas: poloidal profiles of ion saturation current on inner and outer targets

4.1 ICRF results

In Figure 18, one ICRF antennae is shown without the Be screen. The four straps are visible, which can be individually phased.
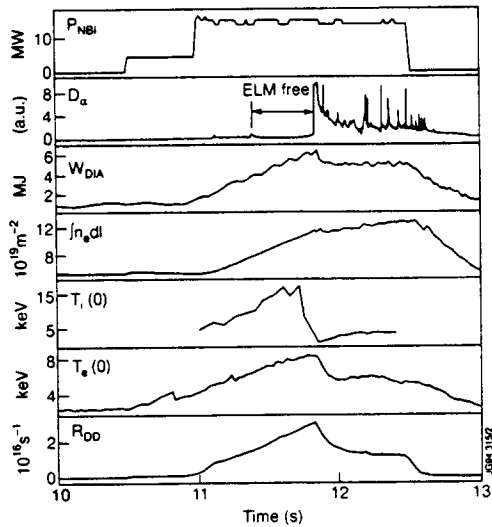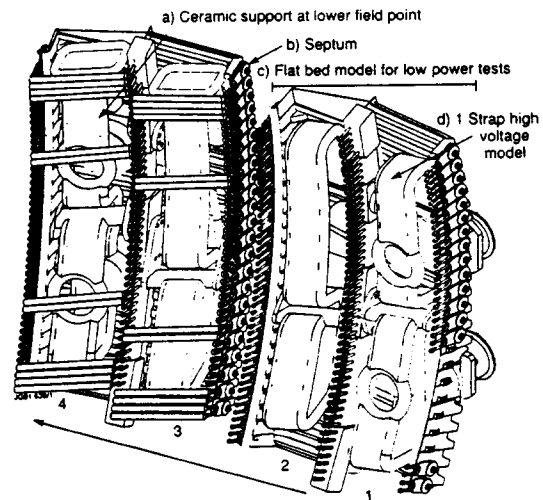

Figure 17. Time evolution of a hot-ion H-mode

Figure 18. New ICRH antenna

The spectrum of the new antennae is shown in Figure 19 for three basic configurations. The basic "monopole" configuration is with 0000 phasing. With $0\pi0\pi$ phasing, a much wider spectrum, extending to higher parallel wavenumber, is produced. With smaller intermediate phase differences between straps, a progressive wave can be produced which will be used for current drive experiments. The first step for FWCD is the observation of direct electron heating, as shown in Figure 20.
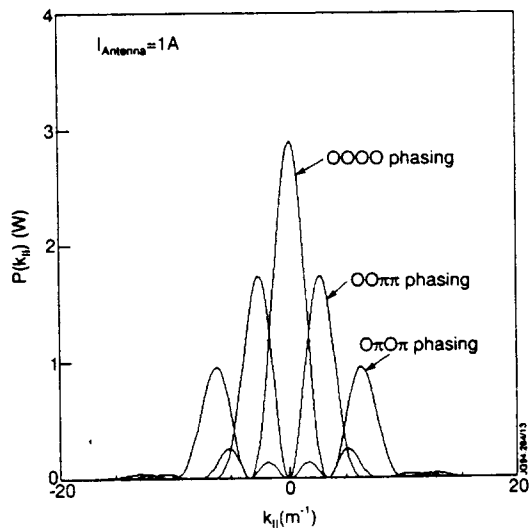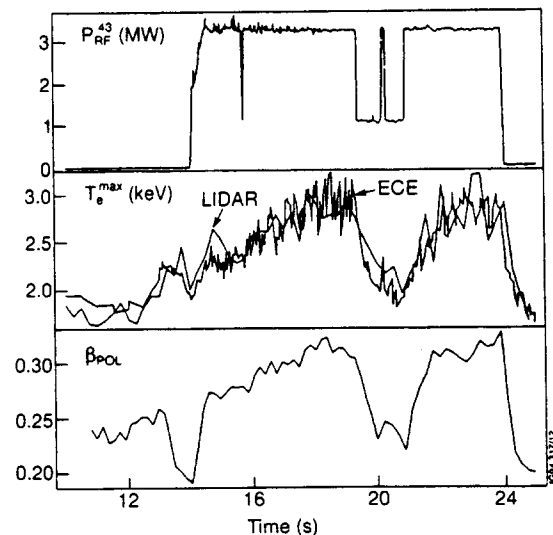

Figure 19. Spectrum of the new antenna

Figure 20. Direct electron heating by ICRF

ICRF power is applied in a situation in which there are no ion resonances in the plasma. Therefore, ion heating can be ruled out, as confirmed by the absence of ion tails in the NPA

11

spectrum. Figure 20 shows that the electron temperature rises in phase with the application of the RF power and so does the poloidal beta, indicating direct electron heating. The main results on the 2MA full current drive are shown in Figure 21.

4.2 LH results

The comparison of the LH current drive efficiency achieved in 1994 and the values obtained in the 1991/92 campaign [4] are shown in Figure 22.
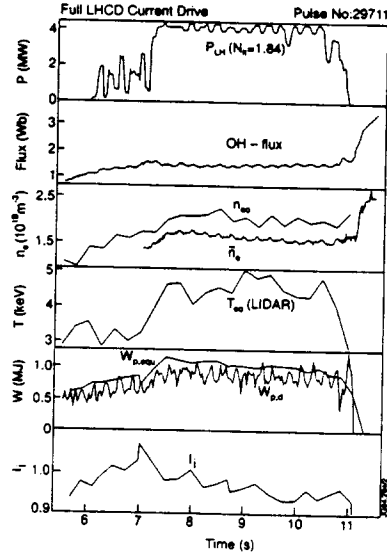
Figure 21. Full 2MA current drive using lower hybrid waves.
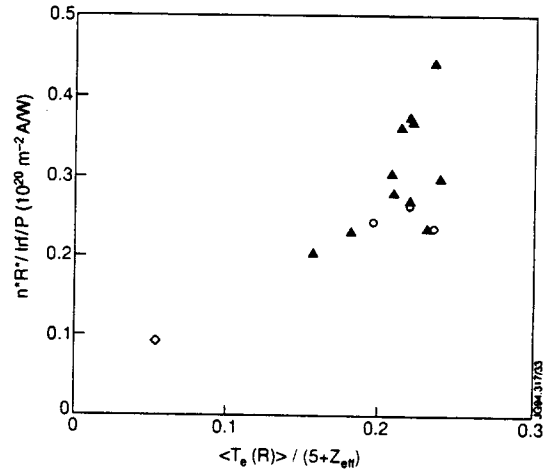
Figure 22. LH current drive efficiency comparison 1991/92 and 1994
Δ - LH alone in 1991/92
▲ - LH + ICRF in 1991/92
o - LH alone in 1994

The current drive efficiency values achieved with LH alone in 1994 are similar to the high values achieved previously with the synergistic effect of combined LH and ICRF power. Sawtooth stabilisation with LH power alone is shown in Figure 23, where the time evolution of central electron temperature is plotted together with LH power for two pulses.

Figure 23. Sawtooth Stabilization with LHCD

12

5. 1994 - 1995 experimental programme

The experimental programme for 1994 and 1995 is based on three main themes:
1. Exploration of the capabilities of the JET pumped divertor;
2. Exploration of high performance plasma regimes;
3. Development of tokamak concept improvement.

In the exploitation of the JET pumped divertor, the main points are, firstly, to compare the performance of a range of divertor configurations, and then, with the use of the divertor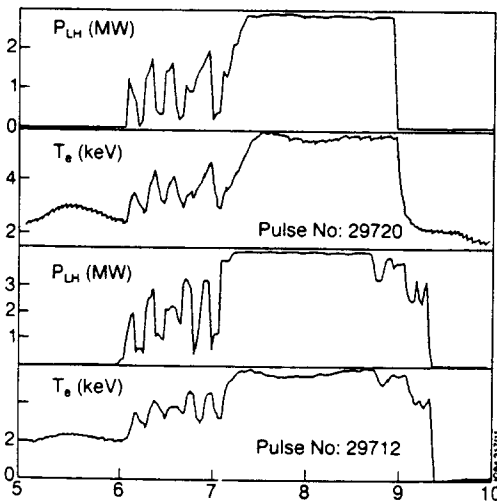 cryopump, to study helium transport and exhaust. With long pulse additional heating, it is planned to investigate steady-state H-modes and to study gas target and radiative divertor regimes. Towards the end of 1994, it is proposed to install beryllium target tiles in the divertor, instead of graphite, and to compare the performance obtained. In addition, JET divertor data will be used for validation of models and extrapolation of physics for Next Step machine and more specifically for ITER [5].

The plans for development of high performance plasmas is centered on development of H-modes to high power with combined ICRF and NB heating, and on the development of H- and VH-mode regimes at high plasma currents (4.5MA). Then, it is proposed to increase the plasma current up to the design value of 6MA, thereby, developing a range of scenarios for the next tritium experiments.

The development of new concepts focusses on the achievement of long stable pulse discharges with a high bootstrap component to the total plasma current, optimizing good confinement at high β_p and high β_n. Prequisites for this work are the achievement of: a large bootstrap fraction plasma, $I_{bs}/I_p > 0.7$; high confinement $H > 3$; and high current drive efficiency. Two main strategies are planned:

i) use transient discharges with high H factor and high β_p and try to replace the current profile obtained during the stable phase with LHCD, FWCD and NBCD to stop the diffusion of the current profile;

ii) Achieve stable configurations, as predicted from theory (for ballooning, infernal, tearing modes): by deep shear reversal with central safety factor $q(0) > 3$ and minimum safety factor $q_{min} \approx 2.4$, using LH current drive during the initial plasma current ramp-up followed by large additional power during the plateau phase.

6. Conclusions

The main achievements during 1994 were the following:
- extensive modifications of the JET device were completed successfully;
- operations have progressed into the exploration of high current and high power plasma regimes in the new divertor configuration;
- the power handling capability of the new divertor has been demonstrated. No "carbon bloom" has been observed;
- H-mode containment has been achieved up to 4MA plasma current, with confinement about twice that in the L-mode regime;
- high performances hot-ion H-modes have been produced;
- full current drive at 2MA, with efficiencies up to $0.25 \times 10^{20} m^{-2} A W^{-1}$, has been obtained.

For the future, it is planned: to reach higher plasma performance by increasing further the plasma current and using the full capabilities of the heating systems; to exploit the full

capabilities of the new divertor in regimes relevant to ITER [4] and for high plasma performance; and to develop further Advanced Tokamak Concept scenarios aimed at the demonstration of a coherent steady-state tokamak. In addition, proposals to extend the JET Programme beyond the presently approved end-date of 1996 are being discussed.

7. References

[1] The JET Project - Design Proposal: EUR-JET-R5 (1976).
[2] Keilhacker, M. and the JET Team, Plasma Physics and Controlled Nuclear Fusion Research, (Würzburg, 1992), IAEA, Vienna, Nuclear Fusion Supplement, Vol **1**, p.15.
[3] JET Team, Nuclear Fusion, **32(2)**, (1992), 187.
[4] Rebut, P-H., Boucher, D., Gambier, D.J., Keen, B.E. and Watkins, M.L., Fusion Engineering and Design, **22** (1993) 7-18.
[5] Tomabechi, K. and the ITER Team, Nucl. Fusion, **31(6)** (1991) 1135.

Appendix I

THE JET TEAM
JET Joint Undertaking, Abingdon, Oxon, OX14 3EA, U.K.

J.M. Adams[1], Y. Agarici[3], P. Ageladarakis, B. Alper, H. Altmann, P. Andrew, S.Ali-Arshad, W. Bailey, B.Balet, Y. Baranov[8], P. Barker, R. Barnsley[2], M. Baronian, D.V. Bartlett, A.C. Bell, G. Benali, E. Bertolini, V. Bhatnagar, A.J. Bickley, H. Bindslev, K. Blackler, D. Bond, T. Bonicelli, K. Borras[13], P. Boucquey, M. Brandon, P. Breger, H. Brelen, W.J. Brewerton, T. Brown, T. Budd, M. Bures, P. Burton, T. Businaro, H. Buttgereit, C. Caldwell-Nichols, D.J. Campbell, D. Campling, P. Card, F. Cecil[24], G. Celentano, C.D. Challis, D. Chiron, J. Christiansen, P. Chuilon, R. Claesen, S. Clement, J.P. Coad, S. Colombi, M. Cooke, S. Cooper, J.G. Cordey, G. Cottrell, M. Cox[7], P. Crawley, O. Da Costa, R. Cusack, G. D'Antona, N. Davies, S.J. Davies, J.J. Davis, H. de Esch, E. Deksnis, N, Deliyanakis, A. Dines, S.L. Dmitrenko, J. Dobbing, N. Dolgetta, S.E. Dorling, P.G. Doyle, H. Duquenoy, A. Edwards, J. Ehrenberg, A. Ekedahl[11], T. Elevant[11], S.K. Erents[7], L.G. Eriksson, H. Falter, A. Fasoli[18], B. Fechner, B. Fischer, G. Fishpool, J. Freiling[15], C. Froger, P. Froissard, K. Fullard, M. Gadeberg, L. Galbiati, M. Garribba, U. Gerstel[13], R. Giannella, A. Gibson, R.D. Gill, R. Goulding[22], A. Gondhalekar, D. Goodall[7], C. Gormezano, N.A. Gottardi, C. Gowers, C. Grisolia[3], H. Guo[23], A. Haigh, C.J. Hancock, P.J. Harbour, N.C. Hawkes[7], N.P. Hawkes[1], J.L. Hemmerich, T. Hender[7], J. Hoekzema, L. Horton, J. How, P.J. Howarth[5], A. Howman, M. Huart, I. Hutchinson[10], T.P. Hughes[4], F. Hurd, B. Ingram, M. Irving, S. Ishida[14], J. Jacquinot, H. Jaeckel, J.F. Jaeger, O.N. Jarvis, F. Jensen, M. Johnson, E.M. Jones, L.P.D.F. Jones, T.T.C. Jones, J-F. Junger, F. Junique, A. Kaye, B.E. Keen, M. Keilhacker, W. Kerner, N.G. Kidd, R. Konig, P. Kupschus, P. Lamalle, R. Lässer, J.R. Last, L. Lauro-Taroni, C. Laviron[3], K. Lawson[7], E. Lazzaro[6], M. Lennholm, J. Lingertat[13], P. Lomas, M. Loughlin, C. Lowry, E. Lyadina, A.C. Maas[15], B. Macklin, C.F. Maggi[16], V. Marchese, F. Marcus, J. Mart, D. Martin, T. Martin, G. Matthews, H. McBryan, G. McCormick[13], A. Meigs, S. Milani, R. Monk[25], P. Morgan, G. Murphy, F. Nave[21], G. Newbert, F. Nguyen[3], P. Nielsen, P. Noll, W. Obert, D. O'Brien, E. Oord, R. Ostrom, M. Ottaviani, S. Papastergiou, V.V. Parail, B. Patel, A. Peacock, N. Peacock[7], R.J.M. Pearce, C. Perry, M.A. Pick, J. Plancoulaine, O. Pogutse, J-P. Poffé, F. Porcelli, L. Porte[19], R. Prentice, S. Puppin, G. Radford[9], T. Raimondi, R. Reichle, S. Richards[12], E. Righi, F. Rimini, A. Rolfe, A. Rookes[12], R.T. Ross, A. Rossi, L. Rossi, R. Russ, G. Sadler, G. Saibene, M. Salisbury[12], G. Sanazzaro, A. Santagiustina, F. Sartori, R. Sartori, P. Savrukhin, M. Schaffer[17], P. Schild, M. Schmid, B. Schunke, S.M. Scott, S. Sharapov, R.L. Shaw, A. Sibley, R. Simonini, A.C.C. Sips, P. Smeulders, R. Smith, F. Söldner, M. Stamp, P. Stangeby[20], D.F. Start, C.A. Steed, D. Stork, P.E. Stott, P. Stubberfield, D. Summers, H. Summers[19], W. Suverkropp, L. Svensson, T. Szabo, M. Tabellini, A. Tanga, A. Taroni, C. Terella, A. Tesini, P.R. Thomas, E. Thompson, K. Thomsen, B. Tubbing, H. van der Beken, E. van der Goot, G. Vayakis, G. Vlases, M. von Hellermann, T. Wade, C. Walker, D. Ward, M.L. Watkins, N. Watkins[1], M.J. Watson, S. Weber, J. Wesson, D. Wilson, T. Winkel, R. Wolf, C. Woodward, I.D. Young, L. Zannelli, N. Zornig, W. Zwingmann.

PERMANENT ADDRESSES

1. UKAEA, Harwell, Didcot, Oxon, UK.
2. University of Leicester, Leicester, UK.
3. CEA, Cadarache, France.
4. University of Essex, Colchester, UK.
5. University of Birmingham, Birmingham, UK.
6. CFP, Milan, Italy.
7. UKAEA Culham Laboratory, Abingdon, Oxon, UK.
8. A.F. Ioffe Institute, St. Petersburg, Russia.
9. Institute of Mathematics, University of Oxford, UK.
10. Massachusetts Institute of Technology, Boston, Mass., USA.
11. Royal Institute of Technology, Stockholm, Sweden.
12. Imperial College, University of London, UK.
13. Max Planck Institut für Plasmaphysik, Garching, Germany.
14. Japan Atomic Energy Research Institute, Naka Fusion Research Laboratory, Ibaraki, Japan.
15. FOM Instituut voor Plasmafysica, Nieuwegein, The Netherlands.
16. Dipartimento di Fisica, University of Milan, Milano, Italy.
17. General Atomics, San Diego, USA.
18. EPFL, Lausanne, Switzerland.
19. University of Strathclyde, 107 Rottenrow, Glasgow, UK.
20. Institute for Aerospace Studies, University of Toronto, Canada.
21. LNETI, Savacem, Portugal.
22. Oak Ridge National Laboratory, Oak Ridge, Tenn., USA.
23. INRS-Energieet Materiaux, Univ. du Quebec, Canada.
24. Colorado School of Mines, Colorado, USA.
25. Royal Holloway College, University of London, UK.

At 1st July, 1994